

MIT Open Access Articles

On the Role of Nanometer Scale Structure on Interfacial Energy

The MIT Faculty has made this article openly available. **Please share** how this access benefits you. Your story matters.

Citation: Kuna, Jeffrey J. et al. "The effect of nanometre-scale structure on interfacial energy." Nat Mater 8.10 (2009): 837-842.

As Published: <http://dx.doi.org/10.1038/nmat2534>

Publisher: Nature Publishing Group

Persistent URL: <http://hdl.handle.net/1721.1/58479>

Version: Author's final manuscript: final author's manuscript post peer review, without publisher's formatting or copy editing

Terms of Use: Article is made available in accordance with the publisher's policy and may be subject to US copyright law. Please refer to the publisher's site for terms of use.



On the Role of Nanometer Scale Structure on Interfacial Energy

¹Jeffrey J. Kuna[†], ¹Kislon Voitchovsky[†], ²Chetana Singh, ²Hao Jiang, ³Steve Mwenifumbo, ²Pradip K. Ghorai, ³Molly M. Stevens, ^{2,4}Sharon C. Glotzer, ¹Francesco Stellacci*

¹Department of Materials Science and Engineering, Massachusetts Institute of Technology, Cambridge, Massachusetts, 02139-4307

²Department of Chemical Engineering, University of Michigan, Ann Arbor, Michigan, 48109-2136

³Department of Materials and Institute for Biomedical Engineering, Imperial College London, London, UK, SW7 2AZ

⁴Department of Materials Science and Engineering, University of Michigan, Ann Arbor, Michigan, 48109-2136

[†]These two authors contributed equally to this work

*Correspondence and requests for materials should be addressed to Francesco Stellacci (frstella@mit.edu).

Abstract

Natural surfaces are often structured with nanometre-scale domains, yet a framework providing a quantitative understanding of how nanostructure affects interfacial energy, γ_{SL} , is lacking. Conventional continuum thermodynamics treats γ_{SL} solely as a function of average composition, ignoring structure. Here we show that, when a surface has domains commensurate in size with solvent molecules, γ_{SL} is determined not only by its average composition but also by a structural component that causes γ_{SL} to deviate from the continuum prediction by a substantial amount, as much as 20% in our system. By contrasting surfaces coated with either molecular (<2 nm) or larger scale domains (>5 nm), we find that while the latter surfaces have the expected linear dependence of γ_{SL} on surface composition, the former exhibit a markedly different non-monotonic trend. Molecular dynamics simulations show how the organization of the solvent molecules at the interface is controlled by the nanostructured surface, which in turn appreciably modifies γ_{SL} .

Interfacial phenomena dominate processes such as protein dynamics¹, heterogeneous catalysis², biological surface activity^{3, 4}, biosensing⁵, self-assembly⁶, and electron transfer⁷. For example, protein functions rely on a well-controlled interface between the protein surface and its surrounding medium^{1, 8}. However, near the protein surface the structure of the liquid is dynamic, making the protein's immediate environment intrinsically difficult to define and experimental investigation challenging. Moreover, the surface structure of biological materials can itself depend on the local liquid environment⁸. Self assembled monolayers^{9, 10} (SAMs) provide a unique opportunity to generate model biological interfaces¹¹. They can have compositions and surface structures that, to a first approximation, resemble biological materials' surfaces but (i) SAMs' structures do not reorganize¹² or denature¹³, and (ii) their composition can be systematically modified, allowing a high degree of control. SAMs on flat surfaces composed of mixtures of immiscible molecules separate into domains of random shape and size (5 nm or larger, Fig. 1 and Fig. 2A)^{12, 14}. However, when SAMs of the same composition are formed on a gold nanoparticle^{15, 16} in a given size range^{17, 18} they separate into striped domains of alternating composition one or two molecules wide (i.e. $\sim 5\text{\AA}$, see Fig. 1 and S9)^{16, 19}. In the nanoparticle case the domains are commensurate with (if not smaller than) the typical hydrophilic or hydrophobic domain size observed on folded proteins, while in the case of flat SAMs the domains are considerably larger.

Interfacial energy γ_{SL} (S=solid, L=liquid, V=vapour) is used to characterize solid-liquid interfaces. It is directly linked to both medias' surface energies (γ_S and γ_L respectively) and to the work of adhesion (W_{SL} , i.e. the free energy cost to separate the media), by the *Dupré* equation²⁰:

$$\gamma_{SL} = \gamma_S + \gamma_L - W_{SL} \quad (1)$$

W_{SL} and γ_{SL} describe the same phenomena and are traditionally measured through contact angle θ_{CA} ²¹.

Current understanding of these interfaces is based on macroscopic observations and relies on the continuum thermodynamic approach (CTA). It is generally accepted that when a surface is made of different components γ_{SL} is the weighted average of the γ_{SL} of the individual components²², leading to a monotonic dependence of θ_{CA} on composition. At a macroscopic scale, line tension, roughness²³, and the presence of macroscopic gas pockets (e.g., air for the lotus leaf effect in Cassie's treatment²⁴) all play a role in determining γ_{SL} ^{25, 26}. However, at the nanoscale, it is not known which surface parameters influence γ_{SL} . Multi-component surfaces in the CTA approach are either treated as uniform or as an ensemble of single component surfaces independently interacting with the liquid²⁷. The range in domain size where one approximation ends and the other begins, or where either cannot be applied, is unknown, yet it is accepted that solvents behave in unique ways when confined or in contact with nanoscale boundaries^{28, 29}. Macroscopic θ_{CA} measurements of mixed SAMs on flat surfaces (> 5 nm domains) have shown that W_{SL} exhibits a monotonic dependence on composition^{22, 30}, and therefore at this length scale the CTA remains valid. However, solubility experiments for mixed SAM-coated nanoparticles (< 2 nm domains) have reported a non-monotonic dependence of saturation concentration on composition, hinting to a failure of the representation of mixing enthalpy in CTA^{15, 31}. At the nanoscale, the only available reports discussing surface structure effects are solely theoretical and address solvent structure but not interfacial energy³². Here, for the first time we present quantitative experimental evidence of an unanticipated and large dependence of W_{SL} (and hence γ_{SL}) not only on composition but also on surface structure using nanopatterned SAMs with domain sizes commensurate with solvent molecules. We use molecular dynamics simulations and experimental findings to corroborate a novel theory that proposes the existence of surface bound half cavities and structure modulated solvent density fluctuations at nanostructured interfaces.

To perform our studies we prepared surfaces coated with binary mixtures of 1-octanethiol (OT) and 6-mercaptohexan-1-ol (MHol) of varying ratios. To obtain ~ 5 nm domains we assembled the molecules directly on flat gold surfaces by immersion in dilute ethanol solutions for one week at room temperature¹⁰ (Fig. 1, Fig. 2A, SI). To generate < 2 nm

domains we first synthesized mixed SAM-coated nanoparticles and then assembled smooth, multilayer films of nanoparticles using layer-by-layer assembly (Fig. 1, SI)³³⁻³⁵. Across compositions we found that the films had very similar thickness and every AFM image acquired had complete coverage of the substrate, with no detectable pinhole defects (Fig. 2B-C, SI Table 1). ANOVA analysis of the roughness values obtained by AFM for slides of different compositions shows no statistically significant variation ($\alpha=0.05$, results summarized in table 1 of SI).

The W_{SL} for these films was measured using macroscopic θ_{CA} and AFM techniques. Because the value for W_{SL} measured by θ_{CA} effectively depends on the area close to the three-phase line³⁶, this technique is intrinsically sensitive to film inhomogeneities or film reconstructions due to the pinning of the solvent droplet. To overcome this problem we relied on measurements performed in liquid with AFM, which allows direct and quantitative probing of local variations in the solvation layer near the surface down to the sub-nanometre level³⁷⁻³⁹, hence allowing for the measurement of interfacial energy in local regions away from the three phase line. Using small amplitude modulation AFM, operated in liquid at amplitudes <2 nm, we were able to simultaneously map the topography of the solid-liquid interface while measuring the energy dissipated by the tip into the interfacial liquid with molecular resolution (Fig. 2B-C, SI, Vořtchovsky et al. in review). Subsequent comparison of the measured local energy dissipation at the interface with that in the bulk liquid allowed us to estimate W_{SL} using a simple model (see SI). Although the AFM-based method bears significant uncertainty due to both experimental and modelling parameters, we always observed a qualitative and statistically significant agreement with the θ_{CA} measurements of W_{SL} (Fig. 2D-E, and SI). Furthermore, whereas the uncertainty associated with AFM measurements is notable in absolute values of W_{SL} , (also because, in the absence of calibration, this technique has a significant linear deviation relative to the CA measurements, see 1F and 2C in SI), such uncertainty is greatly reduced when studying the variation of W_{SL} between different samples imaged under nearly identical experimental conditions (SI). Summarizing, the agreement

between microscopic and nanoscopic measurements allows us to state unequivocally that the effects measured are due to specific nanoscale interactions between the SAMs and the liquid.

The most important results are summarized in Fig. 2D-E. The dependence of W_{SL} on average surface composition follows two markedly different trends when comparing flat and nanoparticle films. For flat SAMs (Fig. 2A, D), we find a monotonic dependence of W_{SL} on composition, as the CTA would predict. For the nanoparticle surfaces, where domains are not wider than 2 nm (Fig. 2B), the trend is clearly non-monotonic (Fig. 2E), and hence the CTA has to be considered inapplicable. In order to substantiate these observations we carried a comprehensive statistical analysis of our data summarized in section 2 of the SI. We find that both the AFM and CA trend for flat SAM are strictly monotonic (R^2 0.413 and 0.940 respectively, see discussion in SI), while the trends for the nanoparticle surfaces are non-monotonic (ANOVA analysis on the residuals after quadratic fitting, $\alpha < 0.01$ in both cases). The largest deviations from the expected linear behaviours are at the 1:2 and 2:1 compositions (20 and 12 mN/m respectively). In addition to the 1:1 composition (discussed below) these two are the compositions where the narrow (in this case < 1.2 nm wide) striped domain morphology is dominant¹⁶; hence these are the compositions where one might expect a stronger effect of structure on interfacial energy. It is worth noting that while in both the flat SAM and the nanoparticle case the actual composition achieved may deviate slightly from the nominal composition used in the SAM preparation, and these deviations may be different for flat and nanoparticle surfaces, the trends are clearly different from each other and it is evident that both cannot be described by the same continuum model. The domain size and local ordering are the only notable differences between the two surfaces and yet the difference in W_{SL} is as large as 20%. The curvature of the nanoparticle cannot explain these observations since the root mean square (RMS) roughness is statistically the same for all mixed ligand nanoparticle films.

These data validate our assumption that a structured surface induces the organization of solvent (as probed by AFM in liquid) whose molecular structure substantially affects W_{SL} , an

intrinsically macroscopic property. We observe a non-monotonic dependence of W_{SL} on composition in water as well as in glycerol (see SI, Fig. S1), suggesting that this behaviour is general. Because we have performed the bulk of our experiments and simulations in water, for clarity of the discussion that follows we use terms specific to water (e.g. hydrophobic) without loss of generalization. We hypothesize that two molecular mechanisms, which we describe in detail below, compete to produce the observed non-monotonic behaviour. To test our hypothesis, we carried out explicit, all-atom molecular dynamics (MD) simulations of striped NPs of different compositions (33%, 50% and 67% MHol, with widths of MHol (OT) stripes of 0.6 (1.2), 0.7 (0.7), and 1.2 (0.6) nm, respectively), surrounded by water molecules (details in SI). The stripe widths were chosen based on the average experimental stripe widths for different compositions. For comparison, we also carried out simulations of ‘Janus’ NPs, on which the two components were completely separated rather than self-assembled into stripes (Fig. S7), but with identical compositions (Fig. S8). The simulations provide access to detailed molecular information to directly investigate both hypothesized mechanisms.

The first hypothesized molecular mechanism draws from the theory of cavitation energies for small, poorly soluble molecules⁴⁰. Cavitation involves the encapsulation by solvent molecules of a hydrophobic solute within an intact but strained hydrogen-bonded cage,⁴⁰⁻⁴¹. For a surface composed of hydrophobic and hydrophilic nanoscale domains, the ‘phobic’ molecules will push the solvent away from the surface while the ‘philic’ molecules will pull the solvent close to the surface. As illustrated in Fig. 3A, on macroscopic domains this should result in two markedly different average distances of the first layers of solvent molecules from the MHol and OT stripes, respectively; this is confirmed by density profiles obtained from our MD simulations on Janus particles shown in Fig 3D. When the hydrophobic domains are small we hypothesize that surface-bound ‘half’ cavities (SBHC) form over them, in analogy to the bulk cavities discussed above. This is illustrated in the cartoon shown in Fig. 3C. SBHCs lower the overall free energy of the entire system, even though they produce strain in the H-bond network surrounding the cavity, causing a corresponding increase in the W_{SL} . In terms of the number of interfacial (< 1.3 nm from NP

surface) water molecules per surfactant, $n_{\text{MHol}}^{\text{W}}$ and n_{OT}^{W} for water immediately over MHol and OT domains, respectively, cavitation will lead to an increase in n_{OT}^{W} and a concomitant decrease in $n_{\text{MHol}}^{\text{W}}$. We note that earlier simulations⁴¹ of water confined between structured flat surfaces reported that hydrophobicity of a small hydrophobic patch, measured in terms of the number density of water molecules above it, decreases when it is surrounded by hydrophilic molecules.

While cavitation is related mainly to the width of the hydrophobic stripes, the second mechanism we propose relates to the width of the hydrophilic stripes. We hypothesize that confinement of solvent molecules within a hydrophilic ‘groove’ of molecular dimensions, as illustrated in Fig. 3C and E, is not favoured entropically, which increases the interfacial free energy and decreases W_{SL} . This will be true for any solvent molecule inside a stripe ‘groove’ especially when the groove walls (neighbouring domains) repel such molecules, and will be critically dependent on the width and depth of the stripe. In Fig. 3A and C we illustrate this concept comparing the entropic freedom (represented by arrows) of two solvent molecules at identical distance from a wetting domain in the case of a flat local surface and that of a stripe groove. For narrow hydrophilic stripes, the effect of this confinement mechanism is strong and becomes weaker as the hydrophilic stripes become wider. A weak confinement means more entropic freedom for solvent molecules in the grooves, hence $n_{\text{MHol}}^{\text{W}}$ will also increase as MHol stripes become wider. Since these two molecular mechanisms – cavitation and confinement – have opposite influences on the W_{SL} , they may lead to a net effect of non-monotonic change of W_{SL} with increasing MHol.

Our simulations confirm the presence of these two competing mechanisms. The inset of Fig. 3C and Fig. S9 show an example of H-bond bridges formed in cavitation. Figs. 3G and H show $n_{\text{MHol}}^{\text{W}}$ and n_{OT}^{W} , respectively, as a function of composition in %MHol. n_{OT}^{W} (Fig. 3H) increases remarkably from 33% to 50% MHol and only slightly from 50% to 67% MHol, supporting our hypothesis that cavitation depends on OT stripe width and increases the water number density over OT end groups. As expected, from 33% to 50% MHol when cavitation is

important, there is a decrease in $n_{\text{MHol}}^{\text{W}}$ due to increasing cavitation. The confinement mechanism is confirmed by comparing $n_{\text{MHol}}^{\text{W}}$ in the case of two particles (50% and 67% MHol) with almost the same hydrophobic stripe width and hence the same degree of cavitation. $n_{\text{MHol}}^{\text{W}}$ changes between these two particles as confinement becomes more pronounced in the narrower stripes. A simplistic way of visualizing this mechanism is that every hydrophobic ‘wall’ (yellow cylinders in Fig. 3C) surrounding the hydrophilic grooves creates an excluded volume for the solvent (white regions in Fig. 3C); the narrower the hydrophilic stripe (red cylinders in Fig. 3C), the larger the fraction of this excluded volume in the total groove volume. In this 50% to 67% MHol range where confinement is important, we see an increase in $n_{\text{MHol}}^{\text{W}}$ (Fig. 3G) associated with increased entropic freedom of water molecules over MHol. Cavitation and confinement are therefore both present in the simulations and since they have opposing effects on W_{SL} we expect that, in combination, they will lead to a non-monotonic dependence of W_{SL} on %MHol.

Based on these findings, we explain the non-monotonic behaviour of the nanoparticles’ W_{SL} as arising from a combination of cavitation and confinement of solvent molecules in the immediate neighbourhood of the nanoparticle. We find that these two mechanisms both depend on stripe width, but oppose each other as the stripe width of the hydrophilic domain increases. The observed non-monotonic behaviour is due to these two contrasting mechanisms (that act on the W_{SL} *per molecule*) combined with the complex way in which domain size in these types of mixed SAMs evolves with composition. The result is a non-monotonic W_{SL} or γ_{SL} dependence on MHol content.

To further validate this interpretation of the data, we measured the effect of ionic strength on W_{SL} . It is known that salts raise the energy needed to form a cavity of a given size⁴². As a consequence the effect of cavitation energy in determining the W_{SL} should become less pronounced as salt concentration is increased, allowing its competing mechanism (confinement) to become more dominant. This implies that the deviations from the linear trend of W_{SL} would have one of two behaviours: either they decrease when large at zero salt

concentration, or they increase when small at zero salt concentration. In the latter case, our interpretation implies that the contrasting mechanisms balance out in de-ionized water, and that this balance is broken at high salt concentration. (At present we can only assume that our second mechanism, solvent confinement, does not vary with ionic strength). We experimentally measured the W_{SL} for our surfaces in DI water and in water containing 3M NaCl. We plotted the deviations of W_{SL} from the expected linear trend in all cases. Figure 4 shows that the results support our hypothesis: when the deviations for DI water are large they become small at the 3M concentration, and vice versa, corroborating the arguments developed through our simulations. It is worth discussing the case of the 50% composition. As discussed above, of the three types of particles studies with a dominant narrow stripe morphology, the 33% and the 67% compositions both showed strong deviations in DI water (20% and 9% respectively) but the 50% did not. However, measurements taken at 3M NaCl (where cavitation is attenuated) demonstrate a strong deviation (14%), pointing to the fact that both mechanisms are strongly present at this composition but only coincidentally cancelling each other. This is to be expected once one accepts the two proposed mechanisms as the 50% composition is the one where both stripes are narrower and hence both effects should be strong.

In summary, our combined experimental and computational results show how the nanoscale structure of a surface affects the local organization of a wetting liquid in such a way as to appreciably modulate the interfacial solvent structure and energy. We see that this unanticipated and large effect is due both to the formation of cavities at the liquid-solid interface, and to confinement of solvent molecules over attractive domains. When combined, these two molecular-level mechanisms produce a non-monotonic wetting dependence on surface composition. This finding has important implications for biological processes where proteins and other biological structures exhibit nanoscale patterning and for our general understanding of solid-liquid interfaces. For instance, these findings show that concepts like hydrophobicity are ill-defined at the nanoscale (and hence possibly for most biological

surfaces) where W_{SL} and thus contact angle measurements depend on nanostructure as much as on chemical composition.

References

1. Bizzarri, A.R. & Cannistraro, S. Molecular Dynamics of Water at the Protein-Solvent Interface. *J. Phys. Chem. B* **106**, 6617-6633 (2002).
2. Hoffmann, M.R., Martin, S.T., Choi, W.Y. & Bahnemann, D.W. Environmental Applications of Semiconductor Photocatalysis. *Chem. Rev.* **95**, 69-96 (1995).
3. Zhdanov, V.P. & Kasemo, B. Kinetics of electrochemical reactions: from single crystals to nm-sized supported particles. *Surf. Sci.* **521**, L655-L661 (2002).
4. Stevens, M.M. & George, J.H. Exploring and engineering the cell surface interface. *Science* **310**, 1135-1138 (2005).
5. Rogers, K.R. Principles of affinity-based biosensors. *Molec. Biotech.* **14**, 109-129 (2000).
6. Willard, A.P. & Chandler, D. The role of solvent fluctuations in hydrophobic assembly. *J. Phys. Chem. B* **112**, 6187-6192 (2008).
7. Oregan, B. & Gratzel, M. A Low-Cost, High-Efficiency Solar-Cell Based on Dye-Sensitized Colloidal TiO_2 Films. *Nature* **353**, 737-740 (1991).
8. Frauenfelder, H., Fenimore, P.W., Chen, G. & McMahon, B.H. Protein folding is slaved to solvent motions. *Proc. Natl. Acad. Sci. U. S. A.* **103**, 15469-15472 (2006).
9. Ulman, A. Formation and structure of self-assembled monolayers. *Chem. Rev.* **96**, 1533-1554 (1996).
10. Love, J.C., Estroff, L.A., Kriebel, J.K., Nuzzo, R.G. & Whitesides, G.M. Self-assembled monolayers of thiolates on metals as a form of nanotechnology. *Chem. Rev.* **105**, 1103-1169 (2005).
11. Mrksich, M. & Whitesides, G.M. Using self-assembled monolayers to understand the interactions of man-made surfaces with proteins and cells. *Annu. Rev. Biophys. Biomol. Struct.* **25**, 55-78 (1996).
12. Stranick, S.J. et al. Nanometer-scale phase separation in mixed composition self-assembled monolayers. *Nanotechnology* **7**, 438-442 (1996).
13. Pace, C.N., Treviño, S., Prabhakaran, E. & Scholtz, J.M. Protein structure, stability and solubility in water and other solvents. *Phil. Trans. Royal Soc. B* **359**, 1225-1235 (2004).
14. Stranick, S.J., Parikh, A.N., Tao, Y.T., Allara, D.L. & Weiss, P.S. Phase-Separation of Mixed-Composition Self-Assembled Monolayers into Nanometer-Scale Molecular Domains. *J. Phys. Chem.* **98**, 7636-7646 (1994).
15. Centrone, A. et al. The role of nanostructure in the wetting behavior of mixed-monolayer-protected metal nanoparticles. *Proc. Natl. Acad. Sci. U. S. A.* **105**, 9886-9891 (2008).
16. Jackson, A.M., Myerson, J.W. & Stellacci, F. Spontaneous assembly of subnanometre-ordered domains in the ligand shell of monolayer-protected nanoparticles. *Nature Mater.* **3**, 330-336 (2004).
17. Singh, C. et al. Entropy-mediated patterning of surfactant-coated nanoparticles and surfaces. *Phys. Rev. Lett.* **99**, 226106 (2007).
18. Carney, R.P. et al. Size limitations for the formation of ordered striped nanoparticles. *J. Am. Chem. Soc.* **130**, 798-799 (2008).
19. Jackson, A.M., Hu, Y., Silva, P.J. & Stellacci, F. From homoligand- to mixed-ligand-monolayer-protected metal nanoparticles: A scanning tunneling microscopy investigation. *J. Am. Chem. Soc.* **128**, 11135-11149 (2006).
20. Dupré, A. Théorie mécanique de la chaleur (Gauthier-Villars, Paris, 1869).
21. θ_{CA} is formed by static, macroscopic liquid droplets at the surface of a flat solid in an inert atmosphere. It provides a direct measurement of W_{SL} through the Young-Dupré equation $W_{SL} = \gamma_{LV} (1 + \cos \theta_{CA}) \approx \gamma_L (1 + \cos \theta_{CA})$:
Young, T. An Essay on the Cohesion of Fluids. *Philos. Trans. Royal Soc.* London (1804).
22. Laibinis, P.E., Fox, M.A., Folkers, J.P. & Whitesides, G.M. Comparisons of Self-Assembled Monolayers on Silver and Gold - Mixed Monolayers Derived from $\text{Hs}(\text{CH}_2)_{21}\text{x}$ and $\text{Hs}(\text{CH}_2)_{10}\text{y}$ (X, Y = CH_3 , CH_2OH) Have Similar Properties. *Langmuir* **7**, 3167-3173 (1991).
23. Wenzel, R.N. Resistance of Solid Surfaces to Wetting by Water. *Industr. & Eng. Chem.* **28**, 988-994 (1936).
24. Barthlott, W. & Neinhuis, C. Purity of the sacred lotus, or escape from contamination in biological surfaces. *Planta* **202**, 1-8 (1997).
25. Chow, T.S. Wetting of rough surfaces. *Journal of Physics-Condensed Matter* **10**, L445-L451 (1998).
26. Gennes, P.G.d. Soft Interfaces (Cambridge University Press, Cambridge, UK, 1994).
27. Cassie A. B. D. , S.B. Wettability of porous surfaces. *Trans. Faraday Soc.* **40**, 546-551 (1944).
28. Bohlen, H., Parry, A.O., Diaz-Herrera, E. & Schoen, M. Intrusion of fluids into nanogrooves. *The European Physical Journal E: Soft Matter and Biological Physics* **25**, 103-115 (2008).
29. Schoen, M. Fluid bridges confined between chemically nanopatterned solid substrates. *Physical Chemistry Chemical Physics* **10**, 223-256 (2008).
30. Imabayashi, S., Gon, N., Sasaki, T., Hobara, D. & Kakiuchi, T. Effect of nanometer-scale phase separation on wetting of binary self-assembled thiol monolayers on Au(111). *Langmuir* **14**, 2348-2351 (1998).

31. It should be noted that solubility is such a complex process depending on numerous factors that singling out any one of them is particularly challenging (see e.g. Maibaum, L. & Chandler, D. Segue Between Favorable and Unfavorable Solvation. *J. Phys. Chem. B* **111**, 9025-9030 (2007)).
32. To the best of our knowledge, there has been to date no discussion of the role of surface structure in determining interfacial energy at solid-liquid interfaces. At the macroscale, the Cassie state of wetting (super-hydrophobicity) could appear to show such structure-dependent effects, but in reality trapped air pockets transform an apparent solid-liquid interface into a mixture of solid-air and solid-liquid interfaces.
33. Shipway, A.N., Katz, E. & Willner, I. Nanoparticle arrays on surfaces for electronic, optical, and sensor applications. *Chemphyschem* **1**, 18-52 (2000).
34. Musick, M.D., Keating, C.D., Keefe, M.H. & Natan, M.J. Stepwise construction of conductive Au colloid multilayers from solution. *Chem. Mater.* **9**, 1499-& (1997).
35. Brust, M., Bethell, D., Kiely, C.J. & Schiffrin, D.J. Self-assembled gold nanoparticle thin films with nonmetallic optical and electronic properties. *Langmuir* **14**, 5425-5429 (1998).
36. Gao, L.C. & McCarthy, T.J. How Wenzel and Cassie were wrong. *Langmuir* **23**, 3762-3765 (2007).
37. O'shea, S.J., Welland, M.E. & Pethica, J.B. Atomic-Force Microscopy of Local Compliance at Solid-Liquid Interfaces. *Chem. Phys. Lett.* **223**, 336-340 (1994).
38. O'Shea, S.J. & Welland, M.E. Atomic force microscopy at solid-liquid interfaces. *Langmuir* **14**, 4186-4197 (1998).
39. Lantz, M., Liu, Y.Z., Cui, X.D., Tokumoto, H. & Lindsay, S.M. Dynamic force microscopy in fluid. *Surf. Interf. Anal.* **27**, 354-360 (1999).
40. Chandler, D. Interfaces and the driving force of hydrophobic assembly. *Nature* **437**, 640-647 (2005).
41. Giovambattista, N., Debenedetti, P.G. & Rossky, P.J. Hydration behavior under confinement by nanoscale surfaces with patterned hydrophobicity and hydrophilicity. *Journal of Physical Chemistry C* **111**, 1323-1332 (2007).
42. Rajamani, S., Truskett, T.M. & Garde, S. Hydrophobic hydration from small to large lengthscales: Understanding and manipulating the crossover. *Proc. Natl. Acad. Sci. U. S. A.* **102**, 9475-9480 (2005).

Supplementary Information accompanies the paper online at <http://www.nature.com/nmat/index.html>

Acknowledgements: F.S. is grateful to the Packard Foundation and to the National Science Foundation CAREER Award (DMR 06-45323) for their generous awards. J.K. was partly supported by a National Science Foundation Graduate Research Fellowship. K.V. acknowledges funding from the Swiss National Science Foundation. C.S., H.J. and S.C.G. acknowledge funding from the National Science Foundation under grant number CTS-0403633. S.M. acknowledges funding from the University of London Central Research Fund, the Institute of Biomedical Engineering, and the Natural Sciences and Engineering Research Council of Canada.

Author contributions: J.K., K.V. and F.S. conceived the experiments. J.K. and S.M. fabricated the nanoparticle films and performed contact angle measurements. J.K. fabricated the large domain films and performed contact angle measurements. K.V. performed AFM measurements and analyzed the AFM data, except roughness measurements (J.K.). J.K., K.V., S.M., M.M.S and F.S. analyzed the experimental data. C.S., H.J., P.G. and S.G. designed the simulations and C.S., H.J. and P.G. analyzed the simulation data. J.K., K.V., C.S., H.J., S.G. and F.S. wrote the majority of the paper. M.M.S and S.M. contributed to manuscript revision.

Competing Interest Statement: The authors declare no competing financial interests.

Figure Legends:

Figure 1: Schematic drawing illustrating the fabrication of the different SAMs studied. Mixed ligand molecules (OT in yellow and MHol in red) are assembled either on flat gold surfaces (flat SAMs) or on gold nanoparticles (see SI for details). On flat SAMs, the ligand mixture self assembles into large (> 5 nm across) homoligand domains. On nanoparticles, the ligands self assemble stripe-like domains < 2 nm wide. Nanoparticle films are then grown by stacking five layers of cross-linked nanoparticles (see SI for details).

Figure 2: SAM-AFM imaging of mixed and homogeneous SAMs in ultrapure water (A-C) and measurement of the corresponding W_{SL} by AFM and CA (D-E). For each image (A-C) the topographic image (left) and the corresponding phase image (right) are presented. The phase image is an indication of the energy dissipated by the vibrating tip in the surface solvation layers and consequently of W_{SL} (see SI). Darker regions in the phase images represent lower local energy dissipation by the tip and hence smaller W_{SL} . For flat SAMs (A), the phase image can distinguish between regions coated with the different ligands (OT is darker and MHol lighter, borderline highlighted). On the nanoparticles, mixed SAMs spontaneously self-assemble into stripes domains (arrows in B), also visible in the corresponding phase image where maxima in the local energy dissipation are visible (lighter regions). Single ligand molecules are resolved, showing structuring and contrast between the different ligand species (arrows). When imaging nanoparticles coated with one ligand, no clear ordering is visible on the nanoparticles (C), as confirmed in the phase image. The W_{SL} for flat SAMs (D) and coated nanoparticles (E) were obtained both from CA (blue) and AFM measurements (red) (see SI for details). Note the different scales for AFM and CA measurements. The variation of W_{SL} with ligand composition is clearly different for the flat SAMs and the nanoparticles, as highlighted by the grey shade in the background of the plots. We notice that the trend implied by that shade is partly a function of the binning of the data. Finer details in-between the compositions studied

here cannot be excluded. Although AFM measurements present a large uncertainty for W_{SL} , there is good qualitative if not quantitative agreement with CA measurements. In the case of flat SAMs (D), the AFM uncertainty is statistically increased by the relatively small sampling area (scan size) compared to the typical homoligand domain sizes. In (B) and (C), the left part of the picture is a simplified cartoon of the coated nanoparticle, serving as a guide for the eye. The contours of the cartoon nanoparticles have also been highlighted. The colour scale (z-scale) is 1 nm, 4 nm and 3 nm for (A), (B) and (C) respectively and 14° , 40° and 40° for the respective corresponding phase images.

Figure 3: Simulation results. (A) Schematic of water density profile and (D) 2D number density profile of water for a 50% MHol Janus nanoparticle with domain sizes commensurate to those of a flat SAM compared with (C) a schematic and (E) the water density profile for a striped 50% MHol nanoparticle. The fuzzy white regions in (C) are cavities bounded by H-bonded water molecules bridging over the OT domains. The fuzzy white region in (A) is an extended empty space over a large hydrophobic region. The hydrogen bond network of waters surrounding this region is irregular and broken. The inset in (C) shows H-bond bridges (see also Fig. S9) anchored to MHol domains (red) and forming over OT domains (yellow). ((B) The region over an OT stripe from the Janus particle and the striped particle is highlighted to evince the role of cavitation in drawing water closer to the hydrophobic surface fraction. (F) Water number density profiles of striped nanoparticles with 33%, 50% and 67% MHol (left to right) composition as a function of radial distance, r , and angular coordinate, θ . The alternating OT and MHol stripes are reflected as the peaks and troughs, respectively, in the density profile as θ is varied for small r . (G,H) Number of interfacial water molecules per ligand head-group over (G) MHol, n_{MHol}^W , and (H) OT, n_{OT}^W , domains, as a function of composition. The error bars reflect the standard deviation of the calculations.

Figure 4: Plot of the deviation of W_{SL} as a function of composition from a linear trend. The deviation was calculated as the difference from the measured W_{SL} and the value expected from a linear trend found using the weighted average of the homoligand nanoparticle films. Increasing the salt concentration increases the work to produce a cavity and decreases the likelihood of cavity formation. With the effect of cavitation thus diminished, the balance with the confinement mechanism is shifted. The values found for the salt solution do not scale proportionally to the values obtained with pure water, indicating effects in addition to the modification of the surface tension of the water are occurring. The error bars reflect the standard deviation of the measurements.

FIG 1

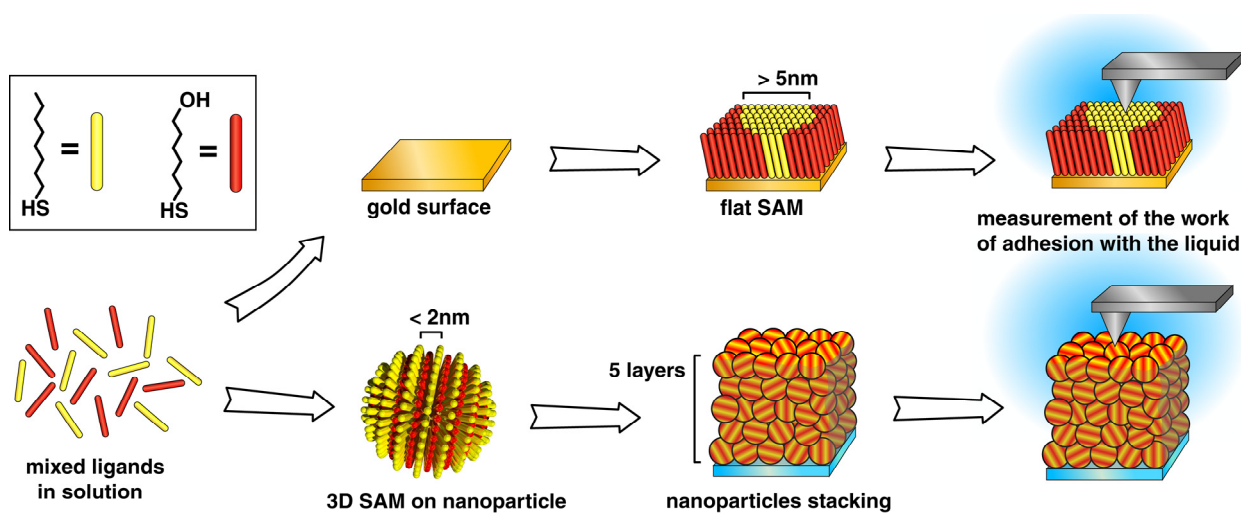


FIG 2

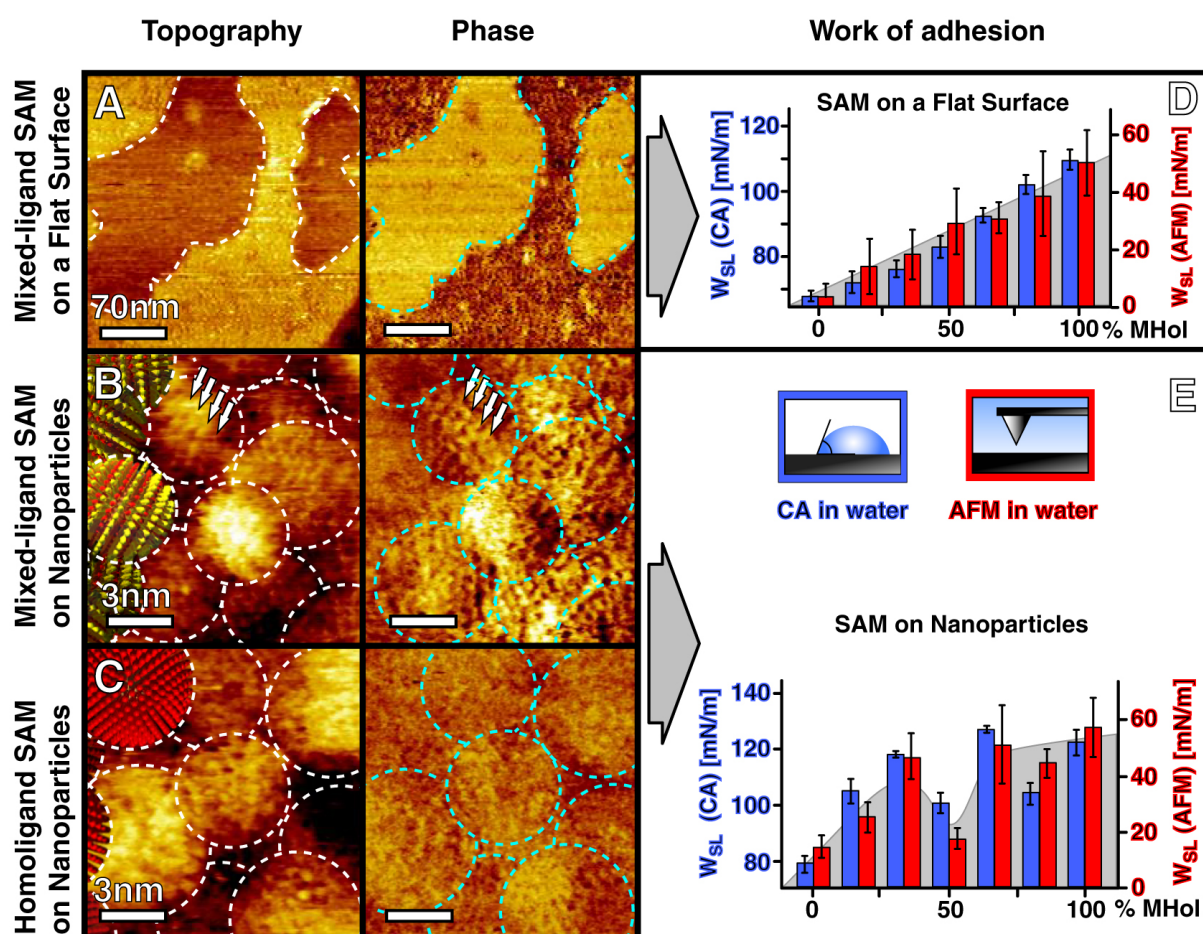


FIG 3

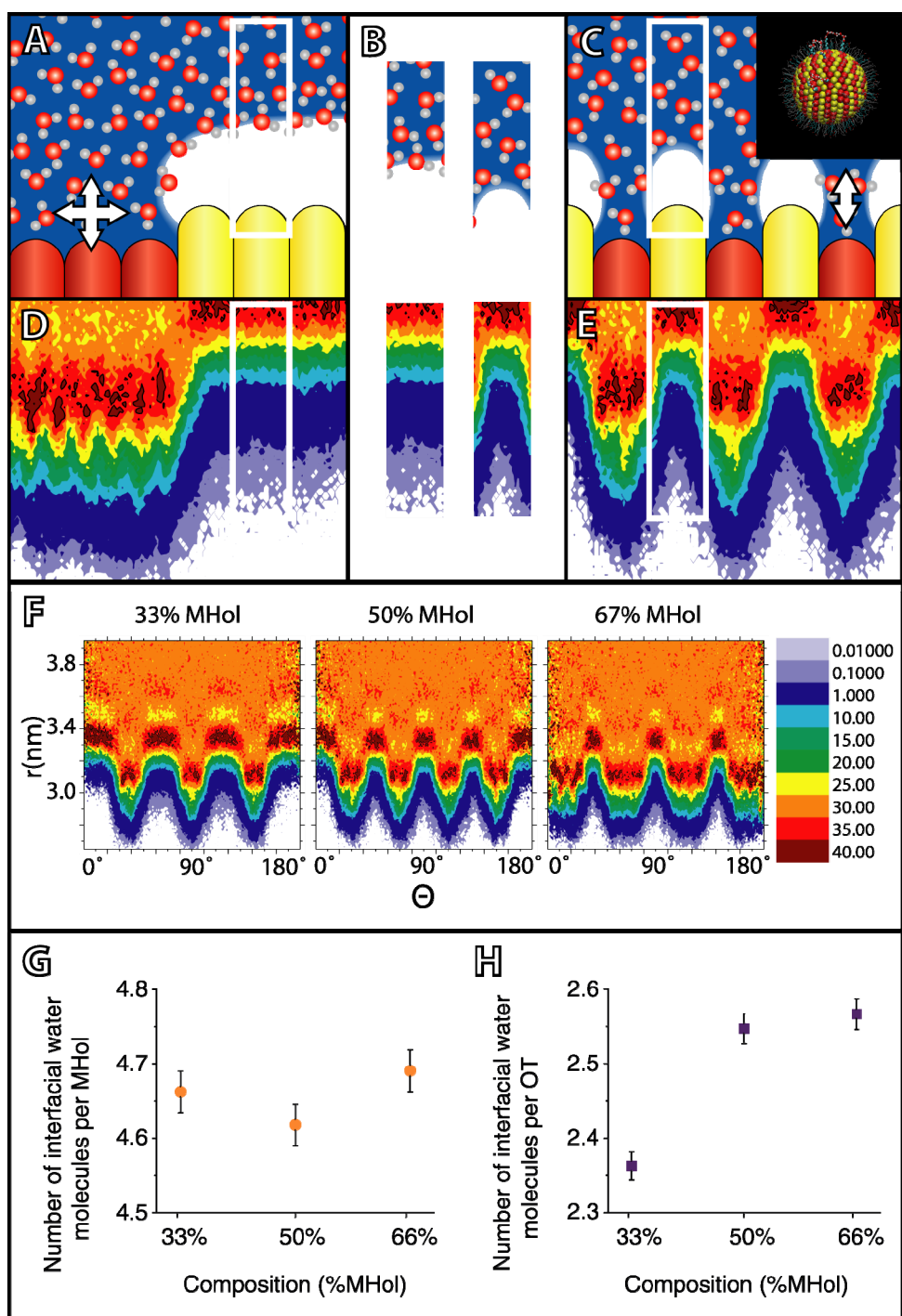


FIG 4

